npj | quantum materials

www.nature.com/npjquantmats

ARTICLE OPEN

Check for updates

Giant Berry curvature dipole density in a ferroelectric Weyl semimetal

Cheng-Long Zhang[1,2,7✉], Tian Liang[3,4,7✉], Yoshio Kaneko[1], Naoto Nagaosa[1,5] and Yoshinori Tokura[1,5,6]

The nonlinear Hall effect (NLHE) reflects Berry-curvature-related properties in non-centrosymmetric but time-reversal-symmetric materials. So far, the NLHE of the investigated systems remains a tiny effect due to the lack of Weyl point as magnetic monopoles in 2D systems or to the high carrier concentration in 3D systems. Here, we report large NLHE due to gigantic Berry curvature dipole density as generated by tilted Weyl cones near the Fermi level in a model ferroelectric Weyl semimetal In-doped $Pb_{1-x}Sn_xTe$. By systematically lowering the carrier concentration down to ~10^{16} cm^{-3}, the Berry curvature dipole density reaches values around 10^{-21} m^3, 10^2–10^7 times higher than the previously reported ones. Furthermore, NLHE exhibits a power law of carrier concentration and follows the k^{-2} relation of the Berry curvature expression derived from the monopole. The present study establishes giant NLHE in a ferroelectric Weyl semimetal, promising for future applications such as current rectification.

npj Quantum Materials (2022)7:103 ; https://doi.org/10.1038/s41535-022-00512-z

INTRODUCTION

The Berry curvature (Ω) in electronic bands of topological quantum materials deeply affects their transport properties[1]. For instance, the Berry curvature contributes to the Hall conductivity via the momentum-space integral over all the occupied states, which results in the anomalous Hall effect (AHE) at zero magnetic field in magnetic materials[2]. Under the time reversal symmetry, however, we cannot observe finite AHE response in nonmagnetic materials at zero magnetic field even though finite Berry curvature exists on electronic band of a crystal lacking in inversion center. Moore and Orenstein[3] realized that the cancellation of Berry curvature contribution, which is enforced by time reversal symmetry, can be removed by driving the system into non-equilibrium state, i.e., external electric field (***E***). In accord with this view, a type of Hall effect with no external magnetic field, namely the nonlinear Hall effect (NLHE), was proposed[4] and experimentally verified[5,6], and more recently observed in various materials without inversion symmetry, including artificially symmetry-broken or interface systems[7–15]. As opposed to the AHE described by the anomalous Hall conductivity, the NLHE is described by the second-order nonlinear susceptibility χ, which is in proportion to the Berry curvature dipole (***D***) defined as $\int_{\boldsymbol{k}} f_0 \frac{\partial \Omega}{\partial \boldsymbol{k}}$ with the Berry curvature Ω and the Fermi distribution function f_0[4]. ***D*** can also be expressed as the contribution from the states near the Fermi surface by the partial integration as $\boldsymbol{D} = \int_{\boldsymbol{k}} \Omega\left(-\frac{\partial f_0}{\partial \boldsymbol{k}}\right) = \int_{\boldsymbol{k}} \Omega \boldsymbol{v}_F\left(-\frac{\partial f_0}{\partial \varepsilon}\right)$ with the Fermi velocity $\boldsymbol{v}_F$. This latter expression indicates that the nonlinear Hall current originates from the shift of the Fermi surface, while the former one stresses more its intrinsic nature. However, these two pictures are equivalent.

The most fundamental structure for emitting the Berry curvature flux is the monopole (Weyl node) in the ***k*** space[16–20], which is described by the relation $\Omega(k) = \pm \frac{\boldsymbol{k}}{2|k|^3}$. Due to the first *k*-derivative nature of the Berry curvature dipole[21], the NLHE is quite different from the AHE, e.g., in the chemical potential dependence, as exemplified by the analytical behaviors when the Fermi level approaches the monopoles. Therefore, the realization of a model Weyl semimetal (WSM) to show the well-defined NLHE is crucial for exploring the fundamental properties of the NLHE. The nonlinear susceptibility χ has two outcomes for the transverse current against the input ac electric field with angular frequency ω: one is the frequency doubling signal (2ω), another is the direct current signal representing the rectification effect[4]. The NLHE is then promising for potential applications in wireless networks and energy harvesting[22–25]. In analogy to the intrinsic magnetic order for the AHE, we then need a corresponding Landau order parameter as the control parameter of the NLHE. Therefore, it is highly demanding to realize a model system for the NLHE coupled strongly with the tunable order parameter that serves as a control knob to turn on/off the NLHE and tune the strength of the inversion symmetry breaking.

In this work, we report on the NLHE of an ideal WSM, In-doped $Pb_{1-x}Sn_xTe$[26,27], which shows the strong coupling with ferroelectric order. We observe sizable NLHE signal appearing along the polar axis, and can be turned on/off by tuning the ferroelectric order through temperature ramping and chemical composition variation. Furthermore, the observed NLHE signal supports a largest value of Berry curvature dipole density reaching as high as 10^{-21} m^3, which characterizes the strength of Berry curvature dipole irrespective of sample dimensions. By tracking the carrier concentration systematically down to ~10^{16} cm^{-3}, we obtain the scaling law between Berry curvature dipole (as well as the effective Berry curvature) and the carrier density. The resultant exponents are found to be consistent with the results calculated based on the simplest model, namely the isolated Weyl monopoles with no other overlapping trivial band dispersions.

[1]RIKEN Center for Emergent Matter Science (CEMS), Wako 351-0198, Japan. [2]Beijing National Laboratory for Condensed Matter Physics, Institute of Physics, Chinese Academy of Sciences, Beijing 100190, People's Republic of China. [3]State Key Laboratory of Low Dimensional Quantum Physics, Department of Physics, Tsinghua University, Beijing, People's Republic of China. [4]Frontier Science Center for Quantum Information, Beijing, People's Republic of China. [5]Department of Applied Physics, University of Tokyo, Tokyo 113-8656, Japan. [6]Tokyo College, University of Tokyo, Tokyo 113-8656, Japan. [7]These authors contributed equally: Cheng-Long Zhang, Tian Liang.
✉email: chenglong.zhang@iphy.ac.cn; tliang@mail.tsinghua.edu.cn

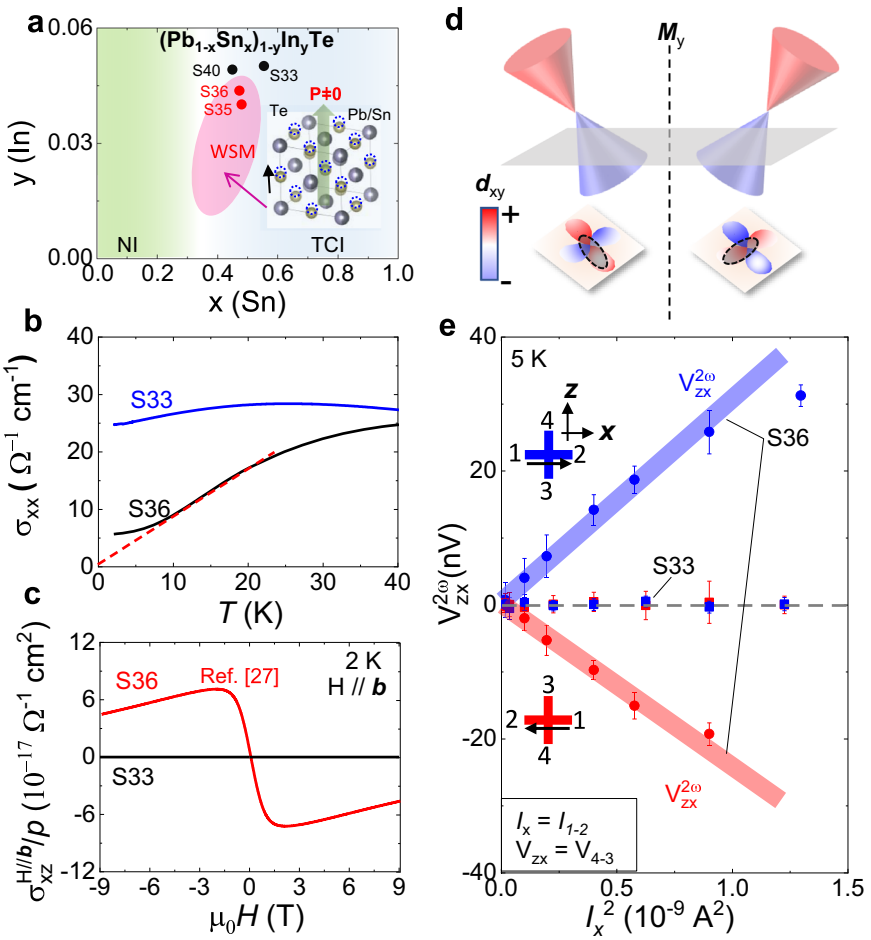

Fig. 1 Nonlinear Hall signals observed in a ferroelectric Weyl semimetal system of $(Pb_{1-x}Sn_x)_{1-y}In_yTe$. a Schematic phase diagram of In-doped PbTe–SnTe; an intermediate Weyl seimimetal (WSM) phase appears between normal insulator (PbTe) and topological crystalline insulator (SnTe) with intrinsic ferroelectric order. Inset shows the distorted structure of WSM phase with polar axis along ***z*** axis. The fully mapped phase diagram with many data points can be found in ref. [26] **b** Temperature-dependent conductivity of the two prototypical samples, S33 and S36. Red linear, dashed line fits conductivity of S36 at temperature below 20 K. **c** In-plane Hall effects measured in S33 and S36 show vanishing and sizable signals, respectively. $\sigma_{xz}^{in\text{-}plane}/p$ of S36 is adapted from ref. [27] **d** The Berry curvature dipole related by the mirror plane displays a certain structure of symmetry of sign, as indicated by the colors of d_{xy}. **e** The nonlinear Hall effect (NLHE) measured for S33 and S36 shows vanishing and sizable signals, respectively. Inset shows the experimental configurations of current and Hall contacts. The error bars represent the standard deviation of the measured data.

RESULTS

Sample and characterization

The highly tunable topological materials system, $(Pb_{1-x}Sn_x)_{1-y}In_yTe$, is engineered by adopting the Murakami's scheme for the WSM phase[18,28,29], where a normal insulator (PbTe) and a topological crystalline insulator (SnTe) are alloyed to access the WSM phase steered by the intrinsic ferroelectric order[26,27,30]. As shown in Fig. 1a, the schematic phase diagram exhibits a hot composition-zone containing the WSM phase with ferroelectric order, while samples out of the hot zone exhibit non-WSM behaviors[27]. The Indium doping (y) is adopted to reduce the bulk carrier concentration, and subsequently to foster the ferroelectric order via reducing the free carrier screening. The ferroelectric transition was evidenced by the temperature-dependent second harmonic generation (SHG) probing the electric polarization as well as by the appearance of a soft phonon mode characteristic of the displacive-type ferroelectrics[27]. The Indium doping becomes more efficient when composition Sn (x) becomes less rich, which makes the regime of WSM tilted with ferroelectric order appearing at Indium (y) concentration in the range of 0.01–0.05, as shown in Fig. 1a. In this study, we use the two prototypical samples, namely S33 ($x = 0.48$, $y = 0.05$; non-WSM without ferroelectric order) and S36 ($x = 0.42$, $y = 0.04$; WSM with ferroelectric order), to explore the NLHE. Figure 1b shows the temperature-dependent dc conductivity of S33 and S36, respectively. The conductivity of S36 exhibits temperature (T)-linear dependence below 20 K where the phonon scattering can be ignored, and Coulomb effects dominate. This is consistent with the proposed formula of the conductivity based on the simplest Weyl model[31]: $\sigma_{dc} = \frac{e^2}{\hbar} * \frac{k_B T}{\hbar v_F(T)} \frac{0.45}{a_T^2 \ln a_T^{-1}}$, where $v_F(T) = v_F\left(\frac{a_0}{a_T}\right)^{\frac{2}{N+2}}$ and $a_T = a_0\left[1 + \frac{(N+2)a_0}{3\pi} \ln\left(\frac{\hbar\Lambda}{k_B T}\right)\right]^{-1}$ are Fermi velocity and renormalized fine structure $\left(a_0 = \frac{e^2}{\hbar} * \frac{1}{4\pi\epsilon v_F}\right)$ with a momentum cutoff Λ. Here, the number of Weyl node monopoles is $N = 16$, while dielectric constant $\epsilon \sim 500$ and $\hbar\Lambda \sim 30$ meV as derived from the optical conductivity data[27]. The T-linear dc conductivity is a typical feature of WSM[31]; which was not accessible in previously reported WSMs due to the overwhelming contribution from trivial bands crossing near the Fermi level. As shown in Fig. 1b, the T-linear fitting to the conductivity of S36 extrapolates to zero conductivity at 0 K, although there is slight deviation due perhaps to the impurity scattering and ferroelectric hysteresis at lower temperatures. The fitting procedure gives Fermi velocity v_F (2 K) $\sim 1.2 \times 10^5$ m/s, which is consistent with the value ($\sim 1.7 \times 10^5$ m/s) we observe in the optical conductivity[27].

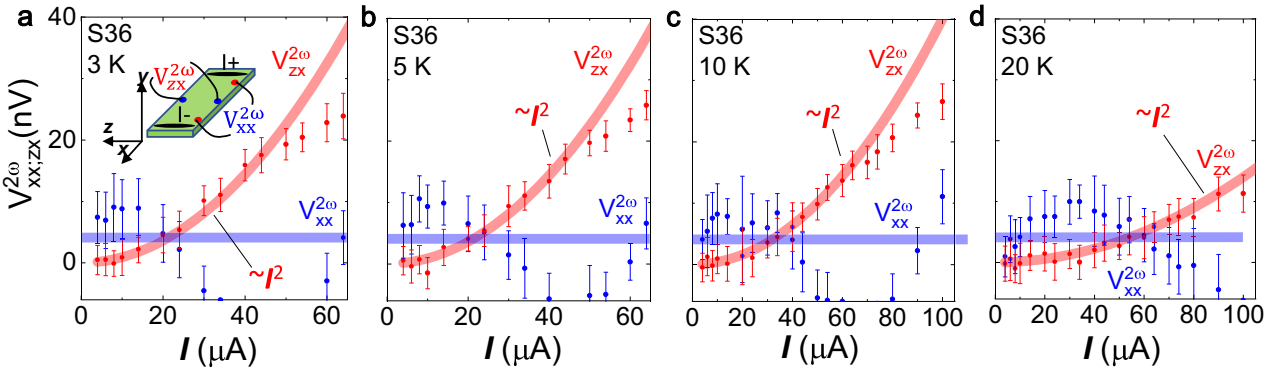

Fig. 2 Temperature dependence of the nonlinear Hall effect. a–d Temperature-dependent 2ω signals in longitudinal and transverse configurations, respectively. Inset shows the contact layout and definition of crystal axes. The nonlinear Hall signal is proportional to the square of excitation current as indicated by shadowed fitting lines, while the longitudinal signals are almost unchanged as indicated by the blue-shadowed lines for eye-guide. The error bars represent the standard deviation of the measured data.

This WSM phase is further confirmed by the in-plane Hall effect[27], which is directly proportional to the weighted Berry curvature expressed as $\Omega \propto \sigma_{xy}^{H//\boldsymbol{b}}/p$. Here the magnetic field is applied along ***b*** (in-plane; we adopt the coordinate relation, ***x***(***a***), ***y***(−***c***), ***z***(***b***) in this paper) direction, and p is the hole-type carrier concentration. The sample S36 exhibits a large weighted Berry curvature in contrast with a vanishing value observed in S33, as shown in Fig. 1c.

Nonlinear Hall effect

Provided the WSM phase with the Berry curvature around the monopoles, it is of great interest to explore the second order effect of the Berry curvature. Figure 1d introduces the simplest model for the Berry curvature dipole to produce the NLHE. The NLHE describes the generation of frequency-doubling current as: $j^{(2\omega)} = \chi_{ijk}E_jE_k$, where the nonlinear susceptibility tensor is $\chi_{ijk} = -\epsilon_{ilk} * \frac{e^3\tau}{2\hbar^2}D_{jl}$; Berry curvature dipole is given by $D_{jl} = \int_k f_0 \frac{\partial\Omega_l}{\partial k_j} = \int_{\boldsymbol{k}} \Omega \boldsymbol{v}_F(-\frac{\partial f_0}{\partial \varepsilon})$ and the Berry curvature dipole density defined as $d_{jl} = \frac{\partial\Omega_l}{\partial k_j}$. Therefore, as shown in Fig. 1d, the d_{xy} exhibits opposite signs in different orthants, and hence the Weyl cone needs tilting to accumulate finite values. Furthermore, the Weyl monopoles, related by the mirror or time reversal symmetry, contribute additively to the total d_{xy}. For the WSM phase in $(Pb_{1-x}Sn_x)_{1-y}In_yTe$, the polar axis is along ***z***, and the Weyl monopoles, associated with slightly tilted Weyl cones due to arbitrary locations of monopoles away from high symmetric ***k*** points[27], are related by the remaining mirror planes and time reversal symmetry, which allows us to use a single Weyl cone model to analyze the observed NLHE signals.

By considering the symmetry constraint (see Supplementary Note 2 for the detailed argument), the ac electric field E_x with the frequency $f = \omega/2\pi$ will produce a 2ω Hall current along ***z*** axis by the χ_{zxx} tensor, with the corresponding Berry curvature dipole D_{xy}. As shown in the inset of Fig. 1e, the current with $f = 13.333$ Hz is fed along ***x*** direction, and the 2ω signal of the NLHE along ***z*** axis is denoted as $V_{zx}^{2\omega}$. As shown in Fig. 1e, $V_{zx}^{2\omega}$ shows sizable signals and depends on the square of the excitation current in the WSM S36 with ferroelectric distortion, while the same measurement produces almost a negligible value in the non-WSM S33. This controlled experiment shows the on/off behaviors of the NLHE directly coupled with the presence/absence of ferroelectricity. We also reverse the current and Hall contacts simultaneously to find $V_{zx}^{2\omega}$ reversed in sign but with the same magnitude, which confirms the nonlinear origin of the second order. Furthermore, we also check another configuration with current fed along ***z*** axis and Hall voltage contacts along ***x*** axis, which should produce no NLHE according to the symmetry analysis (see Supplementary Note 2). As shown in Supplementary Fig. 3, we find the NLHE is much smaller than that along ***z*** axis. Therefore, we conclude that the observed 2ω Hall signal originates from the NLHE produced by the Weyl monopoles.

Temperature dependence of the nonlinear Hall effect

We now investigate the temperature dependence of NLHE, and study the variation of Berry curvature dipole with carrier concentration. As shown in Fig. 2a, $V_{zx}^{2\omega}$ and $V_{xx}^{2\omega}$ in the transverse and longitudinal configuration are monitored simultaneously for sample S36, respectively. We can observe sizable signal of the NLHE $V_{zx}^{2\omega}$, while $V_{xx}^{2\omega}$ remains almost vanishing as expected; the deviation on $V_{zx}^{2\omega}$ as discerned at higher current regime is caused perhaps by thermoelectric signals induced by current-heating effect. Furthermore, no frequency dependence of the NLHE is observed at least in the range of $f = 3$–300 Hz, as shown in Supplementary Fig. 2, confirming negligible thermoelectric effect as a fictious source of nonlinear response. Figures 2a–d show that the NLHE gradually decreases when temperature is raised from 3 to 20 K, while the polar distortion is almost kept constant in this temperature range according to the optical second harmonic generation result in ref. [27] At temperatures higher than 40 K, the NLHE signal (see Supplementary Fig. 4) completely disappears due perhaps to the increase of carrier concentration or change of band tilting, which needs further study to elucidate the origin.

Analysis of the Berry curvature dipole density and scaling law

The nonlinear susceptibility tensor, χ_{ijk}, contains the Berry curvature dipole (***D***) and transport lifetime (τ). Therefore, the carrier concentration and dc conductivity determine the NLHE and hence may cause complicated temperature dependence of the NLHE when the target system has a complicated band structure like conventional WSMs with trivial pockets around the Fermi level. In this context, the target system here is ideal for investigating the purely Weyl monopole based NLHE effect because of the simple band structure composed of the Weyl cones alone near the Fermi level[27]. In order to quantify the NLHE[6], we reformulate the relation as $\chi_{zxx} = \frac{j^{(2\omega)}}{E_x^2} = \frac{E_z^{(2\omega)}}{E_x^2} * \sigma_0$, where σ_0 is the dc conductivity. We can see that the experimental quantity $\frac{E_z^{(2\omega)}}{E_x^2}$ is independent of the relaxation time τand hence the intrinsic quantity for the band structure. More explicitly, $\frac{E_z^{(2\omega)}}{E_x^2} = \frac{e^3\tau}{2\hbar^2}\frac{D_{xy}}{\sigma_{xx}} = \frac{e}{2\hbar^2}\frac{<\Omega_y v_x>}{<v_x^2>}$where < > represents the average with the weight $-\frac{\partial f_0}{\partial \varepsilon}$, which is reduced to the average over the Fermi surface at zero temperature. For the Weyl fermion, the tilting is essential for the nonzero NLHE. When the chemical potential μ is near the Weyl point, there occurs

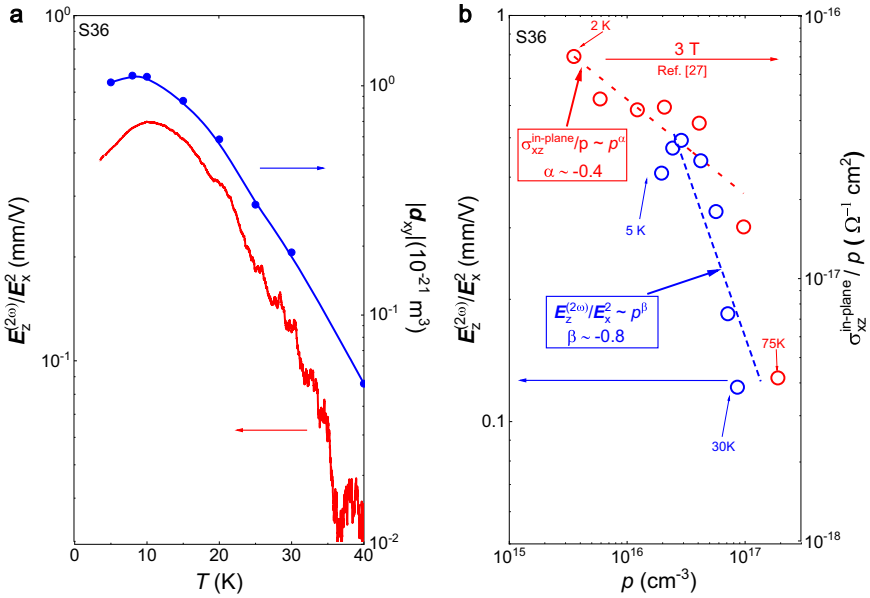

Fig. 3 Temperature- and carrier-density dependence of Berry curvature dipole. a $\frac{E_z^{(2\omega)}}{E_x^2}$ and deduced Berry curvature dipole density d_{xy} versus temperature. **b** $\frac{E_z^{(2\omega)}}{E_x^2}$ and rescaled in-plane Hall effect $\sigma_{xz}^{in\text{-}plane}/p$ are plotted against carrier concentration p. The blue and red dashed lines are the fitting curves to give the estimated exponents, α and β, respectively. Raw data of $\sigma_{xz}^{in\text{-}plane}$ is adapted from ref. [27].

Table 1. The comparison of parameters of the NLHE among different materials.

Materials	Dimension	Carrier density (cm^{-2}/cm^{-3} in 2D/3D)	$E_z^{(2\omega)}/E_x^2$ (m/V)	D_{ij} (Å/ - in 2D/3D)	d_{ij} (m^3)
Bilayer WTe_2[5]	2	~10^{12}	-	~10	~10^{-25}
Few-layer WTe_2[6]	2	~10^{13}	~10^{-9}	~0.1	~10^{-28}
Strained WSe_2[8]	2	~10^{13}	-	~10	~10^{-26}
Twisted WSe_2[9]	2	~10^{12}	~10^{-2}	~1	~10^{-26}
Corrugated graphene[10]	2	~10^{12}	-	~100	~10^{-24}
Bi_2Se_3 surface[11]	2	~10^{13}	~10^{-10}	Extrinsic	-
$LaAlO_3/SrTiO_3$ 2DES[12]	2	~10^{14}	-	~10^3	~10^{-25}
$Ce_3Bi_4Pd_3$[13]	3	~10^{20}	~10^{-3}	~10	~10^{-25}
$TaIrTe_4$[7]	3	~10^{20}	-	~0.1	~10^{-27}
T_d-$MoTe_2$[14]	3	~10^{20}	~0.1	~1	~10^{-26}
α-(BEDT-TTF)$_2I_3$[15]	3	~10^{17}	~10^{-5}	~1	~10^{-23}
$(Pb_{0.58}Sn_{0.42})_{0.96}In_{0.04}Te$ [Current work]	3	~10^{16}	~10^{-3}	~10	~10^{-21}

contributions both from the electrons and holes at finite temperature. In sharp contrast to the linear Hall effect, the contributions to the nonlinear Hall effect from electrons and holes have the same sign, and hence we can regard the carrier density p as that for the shifted μ away from the Weyl point, or the thermally induced carrier density of both electrons and holes when μ is at the Weyl point. In Fig. 3a, the quantity $\frac{E_z^{(2\omega)}}{E_x^2}$ exhibits large enhancement at temperatures below 40 K. According to the Einstein's relation, the conductivity from Weyl cone is $\sigma_0 = \frac{e^2 v_F}{3\pi^2\hbar} * k_F^2 \tau$, and the Berry curvature dipole density is $d_{xy} = \frac{D_{xy}}{p} = \frac{E_z^{(2\omega)}}{E_x^2} * \frac{2\hbar v_F}{e} (3\pi^2 p)^{-\frac{1}{3}}$.Then, d_{xy} can be obtained from experimentally observed quantities, $\frac{E_z^{(2\omega)}}{E_x^2}$, v_F[19] and p. We note that the d_{xy} has no unit dependence on dimension, is a universal physical quantity for representing the strength of Berry curvature dipole effect like the averaged Berry curvature we adopted for AHE[19]. As shown in Fig. 3a, the d_{xy} calculated from experimental values exhibits a large value around 10^{-21} m^3 at low temperatures, which is 10^2–10^7 times higher than the reported values for 2D or 3D systems; Table 1 summarizes to compare the reported values on different materials.

With keeping such a temperature-dependent NLHE in mind, we identify the feature of the NLHE of the present system. In the case of AHE, a useful scheme for unraveling the intrinsic Berry curvature contribution is the so-called Onoda-Nagaosa plot[32], which scales Hall conductivity with longitudinal conductivity. This scaling law was simulated by using a Rashba model with an assumption that the Fermi energy is constant, thus the conductivity as the x-axis variable is dependent only on the impurity scattering time τ. However, topological semimetals usually exhibit very low carrier concentration and strongly temperature-dependent carrier dynamics, which make it difficult to adopt this scheme to study the intrinsic contribution from Berry curvature or its dipoles. Here, to reveal the dominant contribution of intrinsic Berry curvature dipole, we focus on a

scaling scheme for Berry curvature dipole ($\propto \frac{E_z^{(2\omega)}}{E_x^2}$) versus carrier concentration (p), which can be identified in such a system composed of pure monopoles near the Fermi level as the present one. The Fermi level of S36 is close to the monopoles with the energy distance of about $E_F = \hbar k_F v_F \sim 10$ meV, where the Fermi wave vector k_F is estimated from carrier concentration, which will induce large temperature-dependent carrier variation. As show in Fig. 3b, The log–log plot of $\frac{E_z^{(2\omega)}}{E_x^2}$ versus p produces an exponent of $\beta \sim -0.8$ in the form of $\frac{E_z^{(2\omega)}}{E_x^2} \sim p^{\beta}$. This is consistent with the formula $\frac{E_z^{(2\omega)}}{E_x^2} = \frac{\chi_{zxx}}{\sigma_0} \sim <\Omega> \sim \frac{1}{k_F^2} \sim p^{-\frac{2}{3}}$ with assuming a sole $\sim k^{-2}$ Berry curvature contribution from the monopole. This scaling law confirms that the observed NLHE originates from intrinsic Berry curvature dipole around the Weyl monopole, which is the sole Berry curvature flux source in the present system. The scaling of the weighted Berry curvature inferred from the in-plane Hall effect is also plotted against carrier concentration p in Fig. 3b, which produces an exponent $\alpha \sim -0.4$ in the form of $\sigma_{xz}^{\text{in-plane}}/p \sim p^{\alpha}$. This exponent is also roughly in accord with the value ($\alpha = -2/3$) expected from the expression of the monopole, which again confirms that the Berry curvature is dominated by the occupied state of the Weyl cones alone.

DISCUSSION

In conclusion, we have established a model ferroelectric Weyl semimetal system $(Pb_{1-x}Sn_x)_{1-y}In_yTe$ for exploring the NLHE generated by the tilted monopoles. The effective Berry curvature dipole derived from the experimentally observed nonlinear Hall voltage follows a scaling law with carrier concentration, which is consistent with the simplest form of the Berry curvature dipole expected for the Weyl monopoles. Furthermore, the observed Berry curvature dipole density, which characterizes the strength of the NLHE, manifests the largest value as high as 10^{-21} m^3, 10^2–10^7 times higher than the previously reported values, promising for the future applications.

METHODS

Crystal growth and characterizations

Single-crystalline $(Pb_{1-x}Sn_x)_{1-y}In_yTe$ was grown by the conventional vertical Bridgman–Stockbarger technique[18]. Laue and energy dispersion X-ray (EDX) characterizations were performed to determine the crystal axes and specific compositions. The polar axis is determined by the second harmonic generation measurements[19].

Transport measurements

Nonlinear electrical transport measurements were carried out in a Quantum Design physical property measurement system (PPMS) with a multifunctional probe, which is modified to accommodate the coaxial cables. The four-probe method by using the ultrasound indium welding is used for preparing electrodes. For the nonlinear measurements, 2f signals are monitored by the lock-in technique with π/2 phase shift, compared with that of excitation current ($f = 13.333$ Hz).

DATA AVAILABILITY

The data that support the plots within this paper and other findings of this study are available from the corresponding author upon reasonable request.

Received: 11 June 2022; Accepted: 29 September 2022;
Published online: 14 October 2022

REFERENCES

1. Xiao, D., Chang, M.-C. & Niu, Q. Berry phase effects on electronic properties. *Rev. Mod. Phys.* **82**, 1959 (2010).
2. Nagaosa, N., Sinova, J., Onoda, S., MacDonald, A. H. & Ong, N. P. Anomalous Hall effect. *Rev. Mod. Phys.* **82**, 1539 (2010).
3. Moore, J. E. & Orenstein, J. Confinement-induced Berry phase and helicity-dependent photocurrents. *Phys. Rev. Lett.* **105**, 026805 (2010).
4. Sodemann, I. & Fu, L. Quantum nonlinear Hall effect induced by Berry curvature dipole in time-reversal invariant materials. *Phys. Rev. Lett.* **115**, 216806 (2015).
5. Ma, Q. et al. Observation of the nonlinear Hall effect under time-reversal-symmetric conditions. *Nature* **565**, 337–342 (2019).
6. Kang, K., Li, T., Sohn, E., Shan, J. & Mak, K. F. Nonlinear anomalous Hall effect in few-layer WTe_2. *Nat. Mater.* **18**, 324–328 (2019).
7. Kumar, D. et al. Room-temperature nonlinear Hall effect and wireless radiofrequency rectification in Weyl semimetal $TaIrTe_4$. *Nat. Nanotechnol.* **16**, 421–425 (2021).
8. Qin, M.-S. et al. Strain tunable Berry curvature dipole, orbital magnetization and nonlinear Hall effect in WSe_2 monolayer. *Chin. Phys. Lett.* **38**, 017301 (2021).
9. Huang, M. et al. Giant nonlinear Hall effect in twisted WSe_2. Preprint at https://arxiv.org/abs/2006.05615 (2020).
10. Ho, S.-C. et al. Hall effects in artificially corrugated bilayer graphene without breaking time-reversal symmetry. *Nat. Electron.* **4**, 116–125 (2021).
11. He, P. et al. Quantum frequency doubling in the topological insulator Bi_2Se_3. *Nat. Commun.* **12**, 1–7 (2021).
12. Lesne, E. et al. Designing Berry curvature dipoles and the quantum nonlinear Hall effect at oxide interfaces. Preprint at https://arxiv.org/abs/2201.12161 (2022).
13. Dzsaber, S. et al. Giant spontaneous Hall effect in a nonmagnetic Weyl–Kondo semimetal. *Proc. Natl Acad. Sci. USA* **118**, e2013386118 (2021).
14. Tiwari, A. et al. Giant c-axis nonlinear anomalous Hall effect in Td-$MoTe_2$ and WTe_2. *Nat. Commun.* **12**, 1–8 (2021).
15. Kiswandhi, A. & Osada, T. Observation of nonlinear anomalous Hall effect in organic two-dimensional Dirac fermion system. Preprint at https://arxiv.org/abs/2103.00300v2 (2021).
16. Herring, C. Accidental degeneracy in the energy bands of crystals. *Phys. Rev.* **52**, 365 (1937).
17. Volovik, G. E. *The Universe in a Helium Droplet* Vol. 117 (OUP Oxford, 2003).
18. Murakami, S. Phase transition between the quantum spin Hall and insulator phases in 3D: Emergence of a topological gapless phase. *N. J. Phys.* **9**, 356 (2007).
19. Wan, X., Turner, A. M., Vishwanath, A. & Savrasov, S. Y. Topological semimetal and Fermi-arc surface states in the electronic structure of pyrochlore iridates. *Phys. Rev. B* **83**, 205101 (2011).
20. Armitage, N. P., Mele, E. J. & Vishwanath, A. Weyl and Dirac semimetals in three-dimensional solids. *Rev. Mod. Phys.* **90**, 015001 (2018).
21. Zhang, Y., Sun, Y. & Yan, B. Berry curvature dipole in Weyl semimetal materials: An ab initio study. *Phys. Rev. B* **97**, 041101 (2018).
22. Isobe, H., Xu, S.-Y. & Fu, L. High-frequency rectification via chiral Bloch electrons. *Sci. Adv.* **6**, eaay2497 (2020).
23. Zhang, Y. & Fu, L. Terahertz detection based on nonlinear Hall effect without magnetic field. *Proc. Natl Acad. Sci. USA* **118**, e2100736118 (2021).
24. Du, Z. Z., Lu, H.-Z. & Xie, X. C. Nonlinear Hall effects. *Nat. Rev. Phys.* **3**, 744–752 (2021).
25. Ortix, C. Nonlinear Hall effect with time-reversal symmetry: Theory and material realizations. *Adv. Quantum Technol.* **4**, 2100056 (2021).
26. Zhang, C.-L. et al. Highly tunable topological system based on PbTe–SnTe binary alloy. *Phys. Rev. Mater.* **4**, 091201 (2020).
27. Zhang, C.-L. et al. Berry curvature generation detected by Nernst responses in ferroelectric Weyl semimetal. *Proc. Natl Acad. Sci. USA* **118**, e2111855118 (2021).
28. Murakami, S. & Kuga, S. Universal phase diagrams for the quantum spin Hall systems. *Phys. Rev. B* **78**, 165313 (2008).
29. Murakami, S., Hirayama, M., Okugawa, R. & Miyake, T. Emergence of topological semimetals in gap closing in semiconductors without inversion symmetry. *Sci. Adv.* **3**, e1602680 (2017).
30. Liang, T. et al. A pressure-induced topological phase with large Berry curvature in $Pb_{1-x}Sn_xTe$. *Sci. Adv.* **3**, e1602510 (2017).
31. Hosur, P., Parameswaran, S. A. & Vishwanath, A. Charge transport in Weyl semimetals. *Phys. Rev. Lett.* **108**, 046602 (2012).
32. Onoda, S., Sugimoto, N. & Nagaosa, N. Quantum transport theory of anomalous electric, thermoelectric, and thermal Hall effects in ferromagnets. *Phys. Rev. B* **77**, 165103 (2008).

ACKNOWLEDGEMENTS

We thank Y.I. for helpful discussions. T.L. acknowledges the support for the project by the National Key R&D Program of China (No. 2021YFA1401600). This work was partly

supported by CREST (Grant numbers, JPMJCR16F1 & JPMJCR1874) from J.S.T. N.N. was supported also by JSPS KAKENHI Grant Number 18H03676.

AUTHOR CONTRIBUTIONS

C.-L.Z. and Y.T. designed the experiment. C.-L.Z. performed all transport experiments; C.-L.Z. and Y.K. grew the single-crystalline samples and characterized them by EDX; C.-L.Z., T.L., N.N., and Y.T. analyzed the results and wrote the paper. Y.T. conceived the project.

COMPETING INTERESTS

The authors declare no competing interests.

ADDITIONAL INFORMATION

Supplementary information The online version contains supplementary material available at https://doi.org/10.1038/s41535-022-00512-z.

Correspondence and requests for materials should be addressed to Cheng-Long Zhang or Tian Liang.